Influence of hydrodynamic mixing on the distribution of dissolved organic carbon in the East China Sea and the northwest Pacific

Ling Ding[1], Tiantian Ge[1] and Xuchen Wang[1,2,*]

[1] Key Laboratory of Marine Chemistry Theory and Technology, Ministry of Education; Institute of Ocean Studies, Ocean University of China, Qingdao, 266100, China

[2] Center for Isotope Geochemistry and Geochronology, Qingdao National Laboratory for Marine Science and Technology, Qingdao, 266061, China

[*]**Correspondence:** Xuchen Wang (xuchenwang@ouc.edu.cn)

Abstract. Oceanic dissolved organic carbon (DOC) represents one of the largest carbon reservoirs on Earth, and its distribution and behaviour play important roles in carbon cycling and biogeochemical processes in the ocean. We report the distribution and concentrations of DOC for water samples collected from the shelf-edge and slope regions in the East China Sea (ECS) and the Kuroshio Extension (KE) in the northwestern North Pacific (NP) during two cruises in 2014-2015. The DOC concentrations were 45-88 μM in the ECS and 35-65 μM in the KE. In addition to biological processes, the DOC distribution is largely controlled by hydrodynamic mixing of different water masses, while the biological processes are estimated to account for 7% and 8-20% in shaping the DOC distribution in the ECS and KE regions, respectively. By comparing the DOC results with dissolved inorganic carbon (DIC) and dissolved inorganic radiocarbon (Δ^{14}C-DIC) measured from the same water samples, we further

demonstrate that the intrusion of the Kuroshio Current could dilute the DOC concentrations at stations in the outer shelf and slope regions of the ECS. In contrast, the concentrations of DOC in the KE were significantly lower in surface waters than in the ECS, and a relatively low and stable DOC level (~40 μM) was found in deep water (below 1500 m) at all stations. Based on the previously reported DIC and Δ^{14}C-DIC values for the stations, the observed spatial variations of DOC in the upper 700 m among the stations in the KE were mainly influenced by mixing of the two water masses carried by the Kuroshio and Oyashio, the two dominant western boundary currents in the region. The hydrodynamic processes are important factors in the distribution of DOC and carbon cycling and could also have major impacts on primary production and ecosystems in the KE region.

1 Introduction

The world's oceans contain the second largest reservoir of carbon on earth, and dissolved organic carbon (DOC) is the largest reduced carbon pool (685 Pg C) in the ocean (Hansell and Carlson, 1998; Hansell et al., 2009). The DOC in the ocean consists of a highly diverse organic molecular mixture in which ~20,000 individual molecular formulae have been detected (Riedel and Dittmar, 2014). The concentration and distribution of ocean DOC plays significant roles not only in the global carbon cycle but also in control and regulation of the microbial community and many biogeochemical processes in the oceans (Azam et al., 1983; Fenchel, 2008; Carlson et al., 2010; Nelson and Carlson, 2012). Because ocean DOC is directly linked to the oceanic dissolved inorganic carbon (DIC) system through biological photosynthesis and microbial respiration processes, the DOC pool in the ocean also indirectly contributes to the sink of atmospheric CO_2 (Druffel et al., 1992; Carlson et al., 1994; Carlson et al., 1998; Hansell and Carlson, 2001; Carlson et al., 2010).

In the most recent 20 years, improved precision of DOC concentration analysis via the high-

54 temperature catalytic oxidation (HTCO) technique has revealed detailed oceanic DOC
55 distributions, such as those generated by the US Climate Variability Repeat (CLIVAR)
56 hydrography program (Sharp et al., 1995; Sharp et al., 2002; Carlson et al., 2010; Hansell et al.,
57 2012; Bercovici and Hansell, 2016). In general, physical and biological processes combine in
58 modulating the distribution and dynamics of DOC in open oceans (Hansell and Waterhouse,
59 1997; Ogawa et al., 1999; Hansell et al., 2009; Carlson et al., 2010; Bercovici and Hansell,
60 2016). It has been widely observed that oceanic DOC accumulates in the upper water column
61 (100 m) at elevated concentrations (70-90 μM) compared with its relatively constant values
62 (35-45 μM) in deep water (>1000 m), reflecting biological production of DOC in the euphotic
63 zone and microbial consumption with depth (Hansell et al., 2009). However, many previous
64 studies conducted in different coastal and open oceans have shown that the distribution of DOC
65 appeared to depend, to a large extent, on the hydrographical structure and/or horizontal/ vertical
66 water mixing (Hansell and Waterhouse, 1997; Hansell and Peltzer, 1998; Hung et al., 2007;
67 Ogawa et al., 2003; Guo et al., 1995) and the secondary biological forcing superimposed on the
68 physical forcing (Carlson et al., 2010; Wu et al., 2017). Based on a water mixing model, Wu et
69 al. (2017) also reported that microbial degradation contributed 10% of the DOC removal and
70 that physical mixing controlled the majority variation of the DOC pool in the northern South
71 China Sea. In the upper ocean, studies have found that the distribution of DOC often displays
72 obvious latitudinal patterns with relatively higher concentrations (65-85 μM) in the subtropical
73 ocean above 100 m, where stratification might restrict vertical water mixing (Abell et al., 2000;
74 Carlson et al., 2010; Pan et al., 2014). However, in high-latitude oceans, DOC concentrations
75 remain at relatively low levels (45-60 μM) as a result of deep water penetration that dilutes
76 DOC concentrations (Ogawa et al., 1999; Abell et al., 2000; Pan et al., 2014). In the deep ocean,
77 a 14 μM decrease in DOC concentrations occurs along the abyssal circulation pathway from
78 the North Atlantic to the North Pacific Ocean due to differences in thermohaline circulation

patterns (Hansell and Carlson, 1998). Carlson et al. (2010) later confirmed DOC export by the meridional overturning circulation in the Atlantic Ocean and further estimated the export and decay rates of DOC during this water circulation. In addition, concentrations of DOC in the deep Southern Ocean were similar to those in the North Atlantic deep water (NADW) but were higher than in Pacific deep water, which could result from conservative mixing of deep ocean waters from the Atlantic, Indian and Pacific (Bercovici and Hansell, 2016).

The northwestern North Pacific (NP) is a rather special oceanic region where carbon cycling and biogeochemical processes are greatly influenced by two major oceanic western boundary currents: the Kuroshio Current (KC) and Oyashio Current (OC). As one of the largest marginal seas connected to the northwestern NP, the hydrological characteristics of the East China Sea (ECS) are largely influenced by vigorous exchange between the warm saline Kuroshio and cold fresh continental shelf water masses (Hsueh, 2000). Ogawa et al. (2003) reported that the distribution of DOC was primarily controlled by hydrological rather than by biological processes around the shelf edge of the ECS. After exiting the ECS at 30° N/128-129° E, the Kuroshio Current flows northeastward and merges with the southward-flowing Oyashio Current in the mixed water region off the coast of Japan to finally form the Kuroshio Extension (KE) flowing eastward into the North Central Pacific (NCP) (Yasuda et al., 1996; Talley, 1997; Qiu, 2001). The newly formed North Pacific Intermediate Water (NPIW) in the mixed water region has received attention due to its important role in the ocean circulation systems and its impacts on regional carbon cycle and climate variability (Talley, 1993; Hansell et al., 2002; Yasuda, 2003; Wu et al., 2012; Hu et al., 2015). However, few studies have focused on the distribution and dynamics of DOC around the KE region. DOC analysis from different NP stations revealed the export of young DOC accompanied by the NPIW formation, resulting in an enrichment in the Δ^{14}C-DOC values and a reduction in the notably old DOC ^{14}C-age in the Pacific Ocean interior, but the vertical profiles of DOC were only determined at stations in the

subpolar water in the northwestern NP (Hansell et al., 2002). DOC observations in the WOCE (World Ocean Circulation Experiment) and CLIVAR cruises were collected at Line P02 stations along a 30° N latitudinal transect, but the distribution of DOC near the KE was not investigated during these cruises.

Overall, our understanding of DOC dynamics and cycling in the outer shelf and slope regions of the ECS and KE region in the northwestern North Pacific is still limited. In this work, we present the results from DOC concentrations measured in the ECS and Kuroshio Extension (KE) region in the northwestern NP combined with the observations of dissolved inorganic carbon (DIC) concentrations and dissolved inorganic radiocarbon (Δ^{14}C-DIC) values for an evaluation of the roles of the physical mixing process on the distribution of DOC in these two different dynamic oceanic regions.

2 Methods

2.1 Study areas

Water samples were collected from two main oceanic regions: the ECS and the KE region in the northwestern NP (Fig. 1). The ECS is one of the largest marginal seas in the northwest NP, with a broad continental shelf area of approximately 0.5×10^6 km^2 (Gong et al., 2003). In the relatively shallow (< 60 m) and wider inner shelf region, oceanic processes are largely influenced by the inputs of the Yangtze and Yellow Rivers, which are the largest and second largest rivers in China, which together deliver a notably large amount of terrestrial organic matter into the ECS (Wang et al., 2012; Xu et al., 2016). In the outer shelf and slope region of the ECS, the hydrographic characteristics and oceanic processes are affected largely by the northward-flowing Kuroshio Current, which impinges on the shelf break, and a branch that enters the ECS (Chen and Wang, 1999; Guo et al., 2006; Hu et al., 2015; Ge et al., 2016). The high primary productivity and intersection of different water masses make the ECS a complex

region for studying the ocean carbon biogeochemical cycle.

The Kuroshio Extension (KE) in the northwestern NP is an important and highly dynamic region that is largely influenced by the Kuroshio and Oyashio currents. The Kuroshio Current carrying relatively warm and saline waters flows northward along the east coast of Japan, turns eastward near 34° N/140° E, and subsequently flows as the KE into the North Central Pacific (Yasuda et al., 1996; Qiu and Chen, 2011). The southward-flowing Oyashio Current, which carries fresh and cold subarctic water, meets with Kuroshio water at approximately 37° N and forms the Kuroshio-Oyashio inter-frontal zone where the subarctic water mass mixes with the KE water and flows eastward (Yasuda et al., 1996; Qiu and Chen, 2011; Hu et al., 2015). The new NPIW is formed in the same region and is a mixture of relatively fresh and recently ventilated Oyashio water and high-salinity Kuroshio water (Yasuda et al., 1996; Talley, 1997; Qiu and Chen, 2011). The mixed water region in the KE has been characterized as an important sink of anthropogenic CO_2 in the northwestern NP (Tsunogai et al., 1993), and it is a key area for understanding regional climate and ecosystem variations and biogeochemical cycles (Yasuda, 2003; Wu et al., 2012; Hu et al., 2015; Nishibe et al., 2017).

Table 1. Summary of sampling stations and times in the East China Sea (ECS) and the Kuroshio Extension (KE) in the northwestern North Pacific (NP).

Station #	Latitude (°N)	Longitude (°E)	Depth (m)	Sampling Date
ECS				
Stn.1	28.37	126.69	177	12 July 2014
Stn.7	28.30	126.83	265	12 July 2014
Stn.11	28.43	126.53	148	13 July 2014
Z1	28.07	127.13	1078	14 July 2014
Z2	27.93	127.36	1326	14 July 2014
Z4	28.63	127.00	425	14 July 2014
Z3	27.75	126.63	1415	15 July 2014
KE in NP				
K2	25.10	134.02	4100	5 April 2015
B2	37.00	147.00	5586	27 April 2015
B8	30.97	146.99	6000	11-12 April 2015

B9	29.86	146.53	5500	10-11 April 2015
A1-b	32.63	145.95	4800	18 April 2015
A4	34.00	147.80	5800	25 April 2015
A6	34.02	150.04	5800	23 April 2015
A8	34.04	152.02	5500	21 April 2015

146

147 **2.2 Sample collection**

148 Water samples for DOC analysis were collected from 7 stations on the shelf-edge and slope
149 region of the ECS during a cruise in July 2014 onboard the Japanese *R/V Shinset Maru* and
150 from 8 deep stations in the KE region and western NP during a cruise in April-May 2015
151 onboard the Chinese *R/V Dongfanghong-2* (Fig. 1). General information on the sampling
152 stations is summarized in Table 1. All water samples were collected using 12 L Niskin bottles
153 deployed on a rosette with a calibrated SeaBird CTD (model SBE 911) that recorded the
154 temperature and salinity profiles. The accuracies for temperature and salinity are 0.001°C and
155 0.001, respectively.

156 After collection, water samples from the Niskin bottles were transferred directly into a 1 L
157 pre-combusted (at 550°C for 4 h) glass bottle after rinsing three times with seawater. The water
158 was filtered immediately on board through Whatman GF/F filters with 0.7 μM pore size
159 (prebaked at 550°C for 4 h). The filtered water samples were acidified with super-high-purity
160 85% H_3PO_4 (Aladdin®) to pH = 2 and preserved in a frozen state at -20°C until chemical analysis.

161 **2.3 Chemical analysis**

162 Concentrations of DOC were analysed by the high temperature catalytic oxidation (HTCO)
163 method (Sharp et al., 1995; Sharp et al., 2002) using a Shimadzu TOC-L analyser equipped
164 with an ASI-V autosampler. Potassium hydrogen phthalate (KHP) dissolved in high-purity
165 Milli-Q water was used as the DOC standard. The quality assessment for DOC measurements
166 was checked against reference low-carbon water and deep-sea water (CRM Batch 13 with 41-

167 44 μM DOC concentration, supplied by Hansell Biogeochemistry Laboratory at University of
168 Miami, USA). The standard deviation of deep-sea water reference throughout our measuring
169 was ±1 μM, which was used as an index of our analytical precision. The instrumental blank was
170 subtracted using high-purity Milli-Q water that was analysed between samples (before every
171 sample for deep seawater). The average blank of the DOC measurement was ≤ 5 μM, and the
172 analytic precisions on triplicate injections were each ± 3%. All samples were analysed in
173 duplicate from different vials, and the average values were reported. The standard deviation for
174 DOC ranged in ± 0.1- 4.0 μM.

175 The methods for DIC concentrations and Δ^{14}C-DIC measurements were described in detail
176 in separate papers for the samples collected during the same cruises (Ge et al., 2016; Ding et
177 al., 2018). In brief, DIC concentrations were measured using a Shimadzu TOC-L analyser with
178 the total IC mode. Sodium carbonate and sodium bicarbonate dissolved in Milli-Q water were
179 used as the DIC standards, and the concentration values were checked against DIC reference
180 materials (deep sea water) for quality assessment (supplied by Dr Dickson at Scripps Institution
181 of Oceanography). The total blanks were approximately < 0.15% of the seawater DIC
182 concentrations, and the analytic precisions were < 3%. For ^{14}C-DIC measurement, DIC was
183 first extracted as gaseous CO_2 using our modified method with extraction efficiencies > 96%
184 (Ge et al., 2016). The ^{14}C-DIC values were analysed in the National Ocean Sciences Accelerator
185 Mass Spectrometry (NOSAMS) facility at Woods Hole Oceanographic Institution (WHOI).
186 The purified CO_2 was graphed for Δ^{14}C analysis using AMS. The Δ^{14}C values are reported as
187 the modern fraction based on the reference material used (McNichol et al., 1994). The
188 conventional ^{14}C ages (years before present or yr BP) were calculated following the method of
189 Stuiver and Polach (1977). The total uncertainty is 6‰ or better, as tested with a DIC standard
190 (Ge et al., 2016).

191 **3 Results**

3.1 Hydrography

The hydrographic parameters of the sampling stations (temperature and salinity) recorded with the CTD are summarized in Table S1 in the Supporting information, and the depth profiles are plotted in Fig. S1. The hydrology of the water is further described in the T-S diagrams, as plotted in Fig. 2. Because our study involved two distinctive oceanic regions, we separately plotted the hydrographic depth profiles for stations in the ECS and KE regions.

As shown in Fig. 2a and Fig. S1 for the seven shelf-edge and slope stations in the ECS, the water temperature was higher (26.3-29.3°C) at the surface (≤10 m and $\sigma_t \leq 22.1$) and decreased rapidly with depth at all stations. The salinity ranged from 33.88 to 34.87 and exhibited a reversed *S*-shape, i.e., lower at the surface, increasing with depth to the maximum at 150 m water depth (23.2-24.9 σ_t), and decreasing again to 500 m (26.4-26.8 σ_t). The salinity (*S*) remained relatively constant below 500 m depth (at σ_t >26.8) for the three slope stations (Fig. 2a and Fig. S1).

For Sta. K2 and the seven deep stations in the KE, the temperature (*T*) of the surface water ranged from 14.7 to 24.4°C, exhibited a rapid decrease and subsequently remained constant for all stations at density levels of $\sigma_t > 27.6$ at ~1500 m depth (Fig. 2b and Fig. S1). The largest temperature variations occurred in the upper 700 m with the highest *T* (24.4°C) observed at Sta K2 (end *T* value of the Kuroshio water) and the lowest *T* (14.7°C) at Sta B2 observed in the surface layer (5 m) (end *T* values of the Oyashio water) (Fig. 2b). The salinity (*S*) for these stations was higher at the surface, decreased initially to reach a minimum at the density range of 26.4-26.9 σ_t, and subsequently increased with depth to approximately 2500 m with the density layer of 27.6 σ_t (Fig. 2b). The salinity for all stations remained relatively uniform below 2500 m ($\sigma_t > 27.6$). Similar to *T*, the largest differences in salinity also appeared in the upper 700 m water column (the density range of 26.4-27.0 σ_t), where low salinity (34.49) was observed at the surface of Sta B2. The salinity decreased to 33.66 near 250 m and subsequently

increased to values similar to those of the other stations at 2500 m. The salinity for the remaining seven stations (Stas. K2, A1-b, A4, A6, A8, B8 and B9) showed less variation in the surface layers (5 m) (34.76 to 34.98), and Sta K2 had the highest *S* (34.98) at the surface among all stations (Fig. 2b and Fig. S1) (the typical salinity of Kuroshio water is 34.98 and 33.66 for the Oyashio water).

3.2 Concentrations and distribution of DOC

To examine the distribution of DOC with different water masses in the studied regions, we plotted the depth profiles (Fig. 3) and the T-S-DOC diagrams for the ECS and the KE, as shown in Fig. 4. The concentrations of DOC ranged from 45 to 88 μM in the ECS and from 35 to 65 μM in the KE region (Fig. 3 and Table S1). The concentrations of DOC ranged from 55 to 88 μM for the four shelf-edge stations (Stn. 11, 1, 7 and Z4) and from 45 to 84 μM for the three slope stations (Stas. Z1, Z2 and Z3) in the ECS. As plotted in Fig. 3a and Fig. 4a, the concentrations of DOC showed less variation (71-81 μM) in the surface water (≤10 m and $\sigma_t \leq$ 22.1) and decreased rapidly to ~300 m depth for all stations in the ECS. Below 300 m, the concentrations of DOC remained relatively constant down to 1000-1400 m depth for Z1, Z2 and Z3 (Fig. 3a).

In comparison, the concentrations of DOC in the KE region were much lower (43-65 μM) and showed large spatial variations among the stations in the upper 1000 m depth (Fig. 3b). The highest DOC value (65 μM) and the lowest DOC level (43 μM) were measured at the surface at Sta K2 and Sta B2, respectively. In the upper 200 m depth, the concentrations of DOC also showed a notably rapid decrease for most stations. The DOC concentrations were visibly lower at Sta A4 and Sta B2 (36-53 μM) than at the other stations in the upper 700 m depth (at $\sigma_t <$ 27.0), whereas the concentrations were slightly higher in the 500-800 m depth at Sta B8 and Sta A8. The T-S-DOC diagrams showed that DOC concentrations decreased to much lower levels (36-44 μM) at all stations at $\sigma_t > 27.5$ (approximately below 1500 m depth) and remained

constant in deep waters (Fig. 3b and Fig. 4b).

3.3 Concentrations and radiocarbon distribution of DIC

The results of the DIC concentrations and Δ^{14}C-DIC values measured from the same samples have been recently published (Ge et al., 2016; Ding et al., 2018). In this work, we use these data as water mass tracers to support our DOC results. In brief, as shown in Figs. 5a-b, the DIC concentrations were higher in the four shelf-edge stations (Stn.11, Stn.1, Stn.7 and Z4) than that in the slope stations (Z1 and Z2) at the same depths in the ECS (Fig. 5a). The depth profiles of Δ^{14}C-DIC showed a trend opposite to that of the concentrations of DIC, i.e., higher at the surface and decreasing with depth (Fig. 5b). Higher DIC concentrations had lower Δ^{14}C-DIC values. The Δ^{14}C-DIC values at 138 m for Stn.11 and 413 m for Stn. Z4 were significantly lower than the values of the slope stations at the same water depths (Fig. 5b).

The concentrations of DIC were also lower at the surface and increased with depth for the stations in the KE region (Fig. 5c). The large variability in DIC concentrations was observed between 400 and 800 m depths. The Δ^{14}C-DIC values were high at the surface, decreased with depth and showed large variations in the upper 250-1000 m among the stations (Fig. 5d). The Δ^{14}C-DIC values showed a rapid drop in only 300 m of the water column at Sta A4 and in the upper 1000 m depth at Sta B2 and subsequently remained constant below 1000 m depth. The Δ^{14}C-DIC profiles for stations K2, A8, and B9 exhibited a similar trend. The surface bomb ^{14}C signal mixed well down to 600 m and subsequently decreased to 1500 m (1000 m for K2).

4 Discussion

4.1 Processes that control the DOC distribution in the ECS

In this study, the concentrations of DOC measured in the shelf-edge and slope waters are comparable to the values reported previously for the ECS (Hung et al., 2003; Ogawa et al., 2003; Gan et al., 2016). In the shallow shelf region of the ECS, the DOC distributions could be

influenced by many factors such as primary production, bacterial degradation and input from the Yangtze River (Ogawa et al., 2003; Wang et al., 2012; Gan et al., 2016). In the shelf edge and slope region of the ECS, early studies by Hung et al. (2003) and Ogawa et al. (2003) reported that the distribution of DOC was primarily controlled by physical processes rather than production and/or microbial processes. Export of DOC from the shelf water to the slope was also limited because most of the bioavailable DOC had been respired in the shelf waters (Bauer and Bianchi, 2011; Bauer et al., 2013; Ward et al., 2017), and this could be the case, as we observed a statistically positive correlation between DOC and water temperature ($R^2 = 0.82$, $p < 0.001$) for the stations in the ECS (Fig. 6a). A similar pattern has also been found in other marginal seas of the NP (Hung et al., 2007; Dai et al., 2009). In our recent study, we reported that the concentrations of DIC and Δ^{14}C-DIC in the ECS slope and the KE region showed conservative behaviour and could be used as tracers of water mass movement and water parcel homogenization as predicted by the solution mixing model (Ge et al., 2016; Ding et al., 2018). As shown in Fig. 6b, the negative relationship between DOC and DIC ($R^2 = 0.73$, $p < 0.001$) for the stations further suggests that physical processes (such as horizontal and vertical water mixing) influenced the distribution and variation of DOC in the shelf break and slope region of the ECS.

Although the river inputs play an important role in the ECS, our sampling stations are unlikely affected by freshwater input from the Yangtze River, according to the high salinity without any freshwater dilution signals in Fig. 2a and Fig. S1. The vertical variations of DOC for the shelf-edge and slope stations, as shown in Fig. 3a, followed a typical trend similar to the DOC depth profiles observed in open oceans, with higher levels of DOC in the low-density upper waters and low levels of DOC in the high-density deep waters. Around the shelf-edge of the ECS, the vigorous exchange between the warm saline Kuroshio and cold fresh continental shelf water masses could affect the hydrographical characteristics (Hsueh, 2000). As shown in

Fig. 2a, the salinity maximum at the density range of 23.2-24.9 σ_t (near 100-160 m) is influenced largely by the northward-flowing Kuroshio Current. Physical models and chemical tracers both supplied clear evidence of the intrusion of upwelled Kuroshio intermediate water (500-800 m) into the ECS shelf region (Yang et al., 2011; Yang et al., 2012; Ge et al., 2016). To further demonstrate the influence of different water mass mixing processes on the hydrological properties, Figure 7 compared the transectional distributions of density (σ_t), DOC/DIC concentrations and Δ^{14}C-DIC for the seven stations. The cross-section density (σ_t) plot (Fig. 7a) showed that the water mass in the studied area was composed of mixed Kuroshio and shelf waters. It appeared likely that the influences of Kuroshio intermediate water (500-800 m) on the bottom water at station Z4 and Stn. 11 brought low concentrations of DOC, high concentrations of DIC and low Δ^{14}C values of DIC. This intrusion of Kuroshio intermediate water diluted the DOC at Stn. 11 and Z4 (Figs. 7b-d). However, it appears that this upwelling intrusion had almost no effect on the surface water (<100 m depth) for the shelf stations. The intrusion of Kuroshio intermediate water could reflect a smaller-scale or eddy effect rather than a large-scale influence beyond Stn. 11 and Z4 (Ge et al., 2016). In contrast, as shown in Fig. 2a and Fig. 7, the intrusion of the saline Kuroshio water in the density range of 23.2-24.9 σ_t instead of the intermediate Kuroshio water not only contributed to the salinity maximum at approximately 150 m water depth at Stn. 1 and Stn. 7 but also affected the concentrations of DOC/DIC and the DIC-Δ^{14}C values, compared with the upper waters at the other three slope stations (Stas. Z1, Z2 and Z3) influenced largely by the Kuroshio Current (Figs. 7b-d). The river influence and inner shelf export of DOC appeared to be limited in the deep slope stations. At Stn. 1 and Z1, the subsurface DOC maximums were not related to the chlorophyll maximum (data not shown) and could not accumulate in the developed stratification water column, as inferred from the σ_t distribution (Fig. 7a). Previous studies have confirmed that fixed sinking of particulate organic carbon (POC) could partition into the DOC pool, which could result in

316 the subsurface DOC maximum usually observed below the euphotic zone (Druffel et al., 1992;
317 Hansell et al., 2009; Karl et al., 1998).

318 Calculation based on the Δ^{14}C-DIC mass balance showed that approximately 54-65% of the
319 bottom water in the shelf region originated from the intrusion of Kuroshio intermediate water
320 (Ge et al., 2016). If we use the two end-member mixing model as reported by Ge et al. (2016),
321 the conservative concentrations of DOC (referred as DOC^0) could be calculated in the range of
322 61-64 μM, which is slightly higher but comparable to the observed DOC values in the bottom
323 waters at Stn. 11 and Z4 (56-61 μM). The negative values of ΔDOC (measured DOC – DOC^0)
324 could represent the biological consumption effects superimposed on the water physical mixing
325 processes around the shelf-edge and in the slope of ECS. Based on the calculated ΔDOC and
326 the field-measured DOC, we further estimated that the bioavailable fraction of DOC could
327 account for approximately 7% of the total DOC pool in this region. The value is comparable to
328 the results (6.1% and 10% ± 5%) previously reported for the Kuroshio Current and the shelf-
329 slope region of the South China Sea (Gan et al., 2016; Wu et al., 2017). Clearly, biological
330 processes had a significant influence on DOC but were not the dominant controlling factor on
331 the observed DOC distributions in the ECS.

332 **4.2 Processes that influence the DOC profiles in the Kuroshio Extension**

333 In general, the biological and physical processes could combine in control of the DOC
334 profiles in open oceans as well (Hansell and Waterhouse, 1997; Ogawa et al., 1999; Hansell et
335 al., 2009; Carlson et al., 2010; Bercovici and Hansell, 2016). Attributed to the low concentration
336 of nitrate and silicic acid, primary production during spring was low in the KE region (Nishibe
337 et al., 2015). Moreover, notably low levels of available dissolved nitrogen (< 4 μM) were
338 observed in the region (unpublished data) during the same cruise in spring (April-May 2015).
339 The relatively lower surface DOC concentrations (average 57±7 μM) could be due to the low
340 primary production during sampling in the spring season. Despite the low DOC concentrations

in the region, we observed the interesting feature of relatively large spatial variations for DOC concentration among these stations, especially in the upper 1500 m (Fig. 3b and Fig. 4b). For example, concentrations of DOC in the upper 100 m depth at Stas B2 and A4 located north of and around the KE were significantly lower (average 43±5 μM) than those of other stations and were close to the deep water values (ca. 36-44 μM, average 39±3 μM), while elevated concentrations of surface DOC (61-65 μM) prevailed at Sta K2 located far south of KE and the other five stations (54-63 μM, Stas A1-b, B8, B9, A6 and A8), with values 28% higher than average. In the KE region, primary production is largely affected by advection along the KE meander and differs among representative areas in spring, i.e., high in the northern edge and around the KE axis (483-630 mg C m^{-2} day^{-1}), accompanied by high Chl *a* concentration and high column integrated Chl *a* values (35-44 mg m^{-2}) in April (Nishibe et al., 2015). The relatively high primary production should result in a high level of DOC in the stations located north and around the KE, but the measured DOC concentrations were rather low at Stas B2 and A4. In addition, surface mooring data from the NOAA Kuroshio Extension Observatory (KEO) indicated that physical processes dominate the carbon input to the mixed layer at KEO (Fassbender et al., 2017). Therefore, we speculate that the low DOC levels at Sta B2 and A4 were unlikely directly related to the primary production, and instead, the observed large spatial variations were mainly modulated by the mixing dynamics of different water masses rather than biological processes in the region.

Hydrodynamic controls can be directly evaluated by comparing the DOC concentrations with the variables of hydrographic properties. In Figs. 6c and 6d, we examined the correlations of the DOC concentrations with water temperature and DIC concentrations in the KE region, respectively. Overall, a positive relationship exists between the DOC concentrations and temperature in the KE (Fig. 6c, $R^2 = 0.62$, $p < 0.001$), and a negative correlation exists between the DOC and DIC concentrations (Fig. 6d, $R^2 = 0.51$, $p < 0.001$). These observed correlations

of DOC concentrations and hydrographic variables indicate the major role of physical water mixing affecting the DOC distribution in the KE region. To examine the distribution of DOC with different water masses in the KE region, we plotted the DOC and DIC concentrations and Δ^{14}C-DIC values superimposed on the plots of potential temperature (θ) and salinity in Fig. 8. It can be observed that the distributions of DOC, DIC and Δ^{14}C-DIC were clearly associated with different water masses, as identified by the potential water density (σ_0). Higher levels of DOC were associated with lower DIC concentrations, and high Δ^{14}C-DIC values were found in lower density waters ($\sigma_0 < 25.5$, water mass A), while lower levels of DOC were associated with higher DIC concentrations, and low Δ^{14}C-DIC values occurred in denser waters (water mass C and water mass D at $\sigma_0 > 27.1$) (Fig. 8). The denser water mass C with density levels of 26.4-27.1 σ_0 near 500-800 m likely originated from the subarctic gyre, which had low temperature and salinity and was transported by the south-flowing Oyashio Current along the western boundary to the KE region. This water is subsequently mixed with the warm saline water mass transported by the northeast-flowing Kuroshio Current (Fig. 2b and Fig. S1). In contrast, the lower density water mass A with high temperature and salinity corresponding to the six stations (K2, A1-b, A6, A8, B8 and B9) in the south of KE axis was most related to the Kuroshio Current.

Many results suggested that hydrodynamic processes, such as the deep water penetration by vertical mixing, possibly affected the DOC concentrations within the surface waters in the high latitude despite high primary production (Ogawa et al., 1999; Ogawa and Tanoue, 2003). Considering the relatively lower temperature (< 15°C) and salinity (< 34.5) in the upper 700 m (Fig. 2b and Fig. S1), Sta B2 was mainly affected by the intrusion of cold and fresh subarctic water transported by the southward-flowing Oyashio, which also carried lower concentrations of DOC. In contrast, despite the nutrient-depleted and low primary productivity in the subtropical gyre, physical stability factors such as water column stratification could restrict the

vertical mixing of the surface and deep waters, which supplied the environment for DOC accumulation in the surface layer. The relatively higher DOC level in the upper 200 m at Sta K2 was influenced by the northeastward-flowing Kuroshio, which carries a subtropical warm and high-salinity water mass in the upper layers, as demonstrated in Fig. 2b and Fig. S1. The hydrographic properties and DOC profiles of the other five stations (A1-b, B8, B9, A6 and A8) in the KE region showed patterns similar to that of Sta K2, suggesting that the Kuroshio water dominated the mixing at these stations. This observation can be demonstrated more clearly in Fig. 9, where we plotted the salinity, DOC and DIC concentrations, and Δ^{14}C-DIC values for the five stations (B2, A4, A1-b, B8 and B9) as a cross KE transect from north to south. The transectional distributions of salinity could serve as intuitive evidence to show the intrusion of the fresh Oyashio Current, which resulted in the low salinity near 200-800 m (at a density range of 26.4-26.9 σ_t in Fig. 2b). It can be observed that the Kuroshio, which carries relatively high DOC, dominated stations B9, B8 and A1-b from ~200 to 1500 m depth. In contrast, the Oyashio, which carries low salinity, low DOC but high DIC concentrations, and low Δ^{14}C-DIC values in the subarctic intermediate water, influenced the entire water column at Sta B2 and intruded southward, affecting the upper 100-700 m water column of Sta A4, and mixed with the Kuroshio water to form the KE water mass. The unstable mode of the KE could generate active water-mass changes between the south and the north of the KE, thus enhancing meso-scale eddy activities and allowing ocean recirculation formation around the region (Qiu and Chen, 2005; Qiu and Chen, 2011; Ma et al., 2016). This unstable KE mode could transport the fresher Oyashio-origin water southward through meso-scale eddies (Qiu and Chen, 2011), influencing the chemical and biological processes in the KE region. Using the significantly low Δ^{14}C-DIC values at stations B2 and A4 in the upper 700 m depth in the KE region, we also demonstrated the same strong influence of the southward Oyashio-transported subarctic intermediate water mass via meso-scale eddies (Ding et al., 2018). The ratios of Oyashio water to Kuroshio water

mixing for the five stations (B2, B8, A4, A8 and B9) were obtained by mass balance calculations based on the selected two end-member Δ^{14}C-DIC values (an average of 50‰ for the Kuroshio water and -220 ‰ for the NPIW of Oyashio) in the Δ^{14}C-DIC Keeling plot analysis (Fig. 10) (Ding et al., 2018). For example, 55-58% Oyashio water could contribute to produce the observed Δ^{14}C-DIC values at the depth of 500 m in Stas B2 and B8 and 100% Oyashio water at Sta A4 and 96-100% Kuroshio water at Stas A8 and B9, respectively. If we consider that the distribution of DOC is controlled mainly by hydrodynamic mixing in the KE region, the conservative concentrations of DOC could subsequently be calculated using the two water mass mixing model derived from the Δ^{14}C-DIC values within the range of 40-56 μM. The difference between the measured and conservative DOC (DOC^0) concentrations ($\Delta DOC = DOC_{measured} - DOC^0$) can represent other biological processes that secondarily modulate DOC in the KE region. For example, the positive ΔDOC values (~6 μM) that accounted for approximately 11% of the measured DOC at Sta B8 indicated a net DOC increase from biological processes, accompanied by the relatively low DIC concentrations shown in Fig. 9c. The recirculation gyre immediately south of the KE has been found to exhibit high production rates in winter-spring season in the North Pacific due to the entrainment of nutrient-rich water during deep winter mixing (Yasunaka et al., 2013; Yasunaka et al., 2014). However, biological consumptions of DOC could account for 8-20% of the total DOC pool based on the negative ΔDOC values (2-8 μM) and the measured DOC at Stas B2 and A4.

The concentrations of DOC in deep waters in the KE region were low, in the range of 36-44 μM, comparable to the values reported for the deep North Pacific (Druffel et al., 1992; Hansell and Carlson, 1998; Hansell et al., 2009) and the deep South Pacific (34-43 μM) (Doval and Hansell, 2000; Druffel and Griffin, 2015) but slightly lower than the values in the North Atlantic (40-48 μM) (Carlson et al., 2010; Druffel et al., 2016). These uniformly low levels of DOC indicate the homogeneous distribution of deep water and the more presumably refractory DOC

left behind in deeper waters in the KE and North Pacific (Carlson et al., 2010; Hansell et al., 2012; Follett et al., 2014). Radiocarbon measurements of DOC collected in the KE indicate that the ^{14}C age of DOC in deep water was ~6,200 years old (Wang, unpublished data), similar to the DOC ages in the deep NP (Druffel et al., 1992), and support the refractory nature of DOC in the deep KE. The lower deep DOC concentrations in the North Pacific relative to the North Atlantic could be due to the differences in thermohaline circulation patterns, as proposed by Hansell and Carlson (1998), which presented changes in the deep-ocean DOC concentrations along the abyssal circulation pathway. However, by comparing with the deep DOC results in the slope region of the ECS, it can be observed that the deep DOC level in the KE was 10-15 μM lower on average than that in the ECS, implying the possibility of lateral transport of DOC from marginal seas to the ocean interior and cycling in the deep ocean for a long duration.

5 Summary

The results of our study indicate that the concentration of DOC ranged from 45 to 88 μM in the outer shelf and the slope region of ECS and from 35 to 65 μM in the KE region. The distribution of DOC in the shelf-edge and slope region of the ECS was largely controlled by the physical mixing processes of Kuroshio and ECS shelf waters. The upwelling intrusion of Kuroshio intermediate water could dilute the DOC concentrations at stations around the shelf break region of the ECS.

In comparison, the concentrations of DOC in the KE region were significant lower in the surface layer. The DOC in the deep water of the KE had similar comparable values as those reported for the deep north and south Pacific. The large spatial variations of DOC in the upper 700 m among the stations in the KE were influenced primarily by hydrodynamic mixing of two different water masses. The Kuroshio, which carries warm and relatively higher DOC water, and the Oyashio, which carries cold and fresh subarctic intermediate water with lower DOC, mix to form KE. These mixing dynamics could have a major influence on primary production

and on biogeochemical processes in the KE region.

Data availability. All data used in this study will be freely available, for scientific use only, upon request. Anyone interested in using this data set for scientific research should contact the corresponding author via e-mail.

Author contributions. Ling Ding is a post-doc working on this project, participated in the cruises, sample analysis and manuscript writing. Tiantian Ge is a laboratory technician participated in all cruises, sampling and sample analysis. Dr. Xuchen Wang is the corresponding author and leading scientist for this study from proposal writing, cruise and sampling planning, and manuscript writing. All authors have read the manuscript and agreed on the authorship.

Competing interests. The authors declare that they have no conflict of interest.

Acknowledgments. We thank Drs. Lixin Wu and Jing Zhang for providing the ECS and KE cruise opportunity and Drs. Huiwang Gao and Lei Li for the help during sample collection. We thank Yuejun Xue, Chunle Luo, Caili Xu, Yuanzhi Qi and Sen Shan for help and assistance during sample analysis in laboratory. We give our special thanks to the Captains and crew members of *R/V Dongfanghong-2* and *R/V Shinset Maru* for help during the cruises. Financial support for this work was provided by the National Natural Science Foundation of China (grant numbers: 91428101 and 91858210) and the Fundamental Research Funds for the Central Universities (grant number: 201762009).

References

Abell, J., Emerson, S. and Renaud, P.: Distributions of TOP, TON and TOC in the North Pacific subtropical gyre: Implications for nutrient supply in the surface ocean and remineralization in the upper thermocline, J. Mar. Res., 58, 203-222, http://doi.org/10.1357/002224000321511142, 2000.

Azam, F., Fenchel, T., Field, J. G., Gray, J., Meyer-Reil, L. and Thingstad, F.: The ecological role of water-column microbes in the sea, Mar. Ecol Prog Ser., 20, 257-263, 1983.

Bauer, J. E. and Bianchi, T. S.: Dissolved organic carbon cycling and transformation, in: Treatise on Estuarine and Coastal Science, edited by: Wolanski, E. and McLusky, D., 7-67, Academic Press, Waltham, 2011.

Bauer, J. E., Cai, W.-J., Raymond, P. A., Bianchi, T. S., Hopkinson, C. S. and Regnier, P. A. G.: The changing carbon cycle of the coastal ocean, Nature, 504, 61-70, http://doi.org/doi:10.1038/nature 12857, 2013.

Bercovici, S. K. and Hansell, D. A.: Dissolved organic carbon in the deep Southern Ocean: Local versus distant controls, Global Biogeochem. Cycles, 30, 350-360, http://doi.org/10.1002/2015GB005252, 2016.

Carlson, C. A., Ducklow, H. W., Hansell, D. A. and Smith, W. O.: Organic carbon partitioning during spring phytoplankton blooms in the Ross Sea polynya and the Sargasso Sea, Limnol. Oceanogr., 43, 375-386, http://doi.org/10.4319/lo.1998.43.3.0375, 1998.

Carlson, C. A., Ducklow, H. W. and Michaels, A. F.: Annual flux of dissolved organic carbon from the euphotic zone in the northwestern Sargasso Sea, Nature, 371, 405-408, http://doi.org/10.1038/371405 a0, 1994.

Carlson, C. A., Hansell, D. A., Nelson, N. B., Siegel, D. A., Smethie, W. M., Khatiwala, S., Meyers, M. M. and Halewood, E.: Dissolved organic carbon export and subsequent remineralization in the mesopelagic and bathypelagic realms of the North Atlantic basin, Deep-Sea Res. Pt. II, 57, 1433-1445, http://doi.org/10.1016/j.dsr2.2010.02.013, 2010.

Chen, C.-T. A. and Wang, S.-L.: Carbon, alkalinity and nutrient budgets on the East China Sea continental shelf, J. Geophys. Res.: Oceans, 104, 20675-20686, http://doi.org/10.1029/1999jc900055, 1999.

Dai, M., Meng, F., Tang, T., Kao, S.-J., Lin, J., Chen, J., Huang, J.-C., Tian, J., Gan, J. and Yang, S.: Excess total organic carbon in the intermediate water of the South China Sea and its export to the North Pacific, Geochem. Geophys. Geosyst., 10, Q12002, http://doi.org/10.1029/2009GC002752, 2009.

Ding, L., Ge, T., Gao, H., Luo, C., Xue, Y., Druffel, E. R. M. and Wang, X.: Large variability of dissolved inorganic radiocarbon in the Kuroshio Extension of the northwest North Pacific, Radiocarbon, 60, 691-704, http://doi.org/10.1017/RDC.2017.143, 2018.

Doval, M. D. and Hansell, D. A.: Organic carbon and apparent oxygen utilization in the western South Pacific and the central Indian Oceans, Mar. Chem., 68, 249-264, http://doi.org/10.1016/S0304-4203(99)00081-X, 2000.

Druffel, E. R., Williams, P. M., Bauer, J. E. and Ertel, J. R.: Cycling of dissolved and particulate organic matter in the open ocean, J. Geophys. Res., 97, 15639-15659, 1992.

Druffel, E. R. M. and Griffin, S.: Radiocarbon in dissolved organic carbon of the South Pacific Ocean, Geophys. Res. Lett., 42, 4096-4101, http://doi.org/10.1002/2015GL063764, 2015.

Druffel, E. R. M., Griffin, S., Coppola, A. I. and Walker, B. D.: Radiocarbon in dissolved organic carbon of the Atlantic Ocean, Geophys. Res. Lett., 43, 5279-5286, http://doi.org/10.1002/2016GL068746, 2016.

Fassbender, A. J., Sabine, C. L., Cronin, M. F. and Sutton, A. J.: Mixed-layer carbon cycling at the Kuroshio Extension Observatory, Global Biogeochem. Cycles, 31, 272-288, http://doi.org/10.1002/2016GB005547, 2017.

Fenchel, T.: The microbial loop-25 years later, J. Exp. Mar. Bio. Ecol., 366, 99-103, http://doi.org/10.1016/j.jembe.2008.07.013, 2008.

Follett, C. L., Repeta, D. J., Rothman, D. H., Xu, L. and Santinelli, C.: Hidden cycle of dissolved organic carbon in the deep ocean, Proc. Natl. Acad. Sci. USA., 111, 16706-16711, http://doi.org/10. 1073/pnas.1407445111, 2014.

Gan, S., Wu, Y. and Zhang, J.: Bioavailability of dissolved organic carbon linked with the regional carbon cycle in the East China Sea, Deep-Sea Res. Pt. II, 124, 19-28, http://doi.org/10.1016/j.dsr2.2015.06.024, 2016.

Ge, T., Wang, X., Zhang, J., Luo, C. and Xue, Y.: Dissolved inorganic radiocarbon in the Northwest Pacific continental margin, Radiocarbon, 58, 517-529, http://doi.org/10.1017/RDC.2016.23, 2016.

Gong, G.-C., Wen, Y.-H., Wang, B.-W. and Liu, G.-J.: Seasonal variation of chlorophyll a concentration, primary production and environmental conditions in the subtropical East China Sea, Deep-Sea Res. Pt. II, 50, 1219-1236, http://doi.org/10.1016/S0967-0645(03)00019-5, 2003.

Guo, L., Santschi, P. H. and Warnken, K. W.: Dynamics of dissolved organic carbon (DOC) in oceanic environments, Limnol. Oceanogr., 40, 1392-1403, http://doi.org/doi:10.4319/lo.1995.40.8.1392, 1995.

Guo, X., Miyazawa, Y. and Yamagata, T.: The Kuroshio onshore intrusion along the shelf break of the East China Sea: The origin of the Tsushima Warm Current, J. Phys. Oceanogr., 36, 2205-2231, http://doi.org/10.1175/JPO2976.1, 2006.

Hansell, D. A. and Carlson, C. A.: Deep-ocean gradients in the concentration of dissolved organic carbon, Nature, 395, 263-266, http://doi.org/10.1038/26200, 1998.

Hansell, D. A. and Carlson, C. A.: Marine dissolved organic matter and the carbon cycle, Oceanography, 14, 41-49, 2001.

Hansell, D. A., Carlson, C. A., Repeta, D. J. and Schlitzer, R.: Dissolved organic matter in the ocean: A controversy stimulates new insights, Oceanography, 22, 202-211, http://doi.org/10.5670/oceanog.2009.109, 2009.

Hansell, D. A., Carlson, C. A. and Schlitzer, R.: Net removal of major marine dissolved organic carbon fractions in the subsurface ocean, Global Biogeochem. Cycles, 26, GB1016, http://doi.org/10.1029/2011gb004069, 2012.

Hansell, D. A., Carlson, C. A. and Suzuki, Y.: Dissolved organic carbon export with North Pacific Intermediate Water formation, Global Biogeochem. Cycles, 16, 1007, http://doi.org/10.1029/2000GB001361, 2002.

Hansell, D. A. and Peltzer, E. T.: Spatial and temporal variations of total organic carbon in the Arabian Sea, Deep-Sea Res. Pt. II, 45, 2171-2193, http://doi.org/doi:10.1016/S0967-0645(98)00067-8, 1998.

Hansell, D. A. and Waterhouse, T. Y.: Controls on the distributions of organic carbon and nitrogen in the eastern Pacific Ocean, Deep-Sea Res. Pt. I, 44, 843-857, http://doi.org/10.1016/S0967-0637(96)00128-8, 1997.

Hsueh, Y.: The Kuroshio in the East China Sea, J. Mar. Syst., 24, 131-139, http://doi.org/10.1016/S0924-7963(99)00083-4, 2000.

Hu, D., Wu, L., Cai, W., Gupta, A. S., Ganachaud, A., Qiu, B., Gordon, A. L., Lin, X., Chen, Z., Hu, S., Wang, G., Wang, Q., Sprintall, J., Qu, T., Kashino, Y., Wang, F. and Kessler, W. S.: Pacific western boundary currents and their roles in climate, Nature, 522, 299-308, http://doi.org/10.1038/nature14504, 2015.

588 Hung, J. J., Chen, C. H., Gong, G. C., Sheu, D. D. and Shiah, F. K.: Distributions, stoichiometric patterns
589 and cross-shelf exports of dissolved organic matter in the East China Sea, Deep-Sea Res. Pt. II, 50,
590 1127-1145, http://doi.org/10.1016/S0967-0645(03)00014-6, 2003.
591 Hung, J. J., Wang, S. M. and Chen, Y. L.: Biogeochemical controls on distributions and fluxes of
592 dissolved and particulate organic carbon in the Northern South China Sea, Deep-Sea Res. Pt. II, 54,
593 1486-1503, http://doi.org/10.1016/j.dsr2.2007.05.006, 2007.
594 Karl, D. M., Hebel, D. V., Björkman, K. and Letelier, R. M.: The role of dissolved organic matter release
595 in the productivity of the oligotrophic North Pacific Ocean, Limnol. Oceanogr., 43, 1270-1286,
596 http://doi.org/doi:10.4319/lo.1998.43.6.1270, 1998.
597 Ma, X., Zhao, J., Chang, P., Liu, X., Montuoro, R., Small, R. J., Bryan, F. O., Greatbatch, R. J., Brandt,
598 P., Wu, D., Lin, X. and Wu, L.: Western boundary currents regulated by interaction between ocean
599 eddies and the atmosphere, Nature, 535, 533-537, http://doi.org/10.1038/nature18640, 2016.
600 McNichol, A. P., Jones, G. A., Hutton, D. L., Gagnon, A. R. and Key, R. M.: The rapid preparation of
601 seawater $\sum CO_2$ for radiocarbon analysis at the National Ocean Sciences AMS Facility, Radiocarbon,
602 36, 237-246, 1994.
603 Nelson, C. E. and Carlson, C. A.: Tracking differential incorporation of dissolved organic carbon types
604 among diverse lineages of Sargasso Sea bacterioplankton, Environ Microbiol., 14, 1500-1516,
605 http://doi.org/10.1111/j.1462-2920.2012.02738.x, 2012.
606 Nishibe, Y., Takahashi, K., Sato, M., Kodama, T., Kakehi, S., Saito, H. and Furuya, K.: Phytoplankton
607 community structure, as derived from pigment signatures, in the Kuroshio Extension and adjacent
608 regions in winter and spring, J Oceanogr., 73, 463-478, http://doi.org/10.1007/s10872-017-0415-3,
609 2017.
610 Nishibe, Y., Takahashi, K., Shiozaki, T., Kakehi, S., Saito, H. and Furuya, K.: Size-fractionated primary
611 production in the Kuroshio Extension and adjacent regions in spring, J Oceanogr., 71, 27-40, http://
612 doi.org/10.1007/s10872-014-0258-0, 2015.
613 Ogawa, H., Fukuda, R. and Koike, I.: Vertical distributions of dissolved organic carbon and nitrogen in
614 the Southern Ocean, Deep-Sea Res. Pt. I, 46, 1809-1826, http://doi.org/10.1016/S0967-0637(99)
615 00027-8, 1999.
616 Ogawa, H. and Tanoue, E.: Dissolved Organic Matter in oceanic waters, J Oceanogr., 59, 129-147,
617 http://doi.org/10.1023/a:1025528919771, 2003.
618 Ogawa, H., Usui, T. and Koike, I.: Distribution of dissolved organic carbon in the East China Sea, Deep-
619 Sea Res. Pt. II, 50, 353-366, http://doi.org/10.1016/S0967-0645(02)00459-9, 2003.
620 Pan, X., Achterberg, E. P., Sanders, R., Poulton, A. J., Oliver, K. I. C. and Robinson, C.: Dissolved
621 organic carbon and apparent oxygen utilization in the Atlantic Ocean, Deep-Sea Res. Pt. I, 85, 80-87,
622 http://doi.org/10.1016/j.dsr.2013.12.003, 2014.
623 Qiu, B.: Kuroshio and Oyashio currents, in: Encyclopedia of Ocean Science, edited by: Steele, J. H.,
624 Turekian, K. K. and Thorpe, S. A., 1413–1425, Academic Press, San Diego, 2001.
625 Qiu, B. and Chen, S.: Variability of the Kuroshio Extension Jet, recirculation gyre, and mesoscale eddies
626 on decadal time scales, J. Phys. Oceanogr., 35, 2090-2103, http://doi.org/10.1175/jpo2807.1, 2005.
627 Qiu, B. and Chen, S.: Effect of decadal Kuroshio Extension Jet and eddy variability on the modification
628 of North Pacific Intermediate Water, J. Phys. Oceanogr., 41, 503-515, http://doi.org/10.1175/
629 2010JPO4575.1, 2011.
630 Riedel, T. and Dittmar, T.: A method detection limit for the analysis of natural organic matter via Fourier
631 Transform Ion Cyclotron Resonance Mass Spectrometry, Anal Chem., 86, 8376-8382, http://doi.org
632 /10.1021/ac501946m, 2014.
633 Sharp, J. H., Benner, R., Bennett, L., Carlson, C. A., Fitzwater, S. E., Peltzer, E. T. and Tupas, L. M.:

Analyses of dissolved organic carbon in seawater: the JGOFS EqPac methods comparison, Mar. Chem., 48, 91-108, http://doi.org/10.1016/0304-4203(94)00040-K, 1995.
Sharp, J. H., Carlson, C. A., Peltzer, E. T., Castle-Ward, D. M., Savidge, K. B. and Rinker, K. R.: Final dissolved organic carbon broad community intercalibration and preliminary use of DOC reference materials, Mar. Chem., 77, 239-253, http://doi.org/10.1016/S0304-4203(02)00002-6, 2002.
Stuiver, M. and Polach, H. A.: Discussion reporting of ^{14}C data, Radiocarbon, 19, 355-363, http://doi.org/10.1017/S0033822200003672, 1977.
Talley, L. D.: Distribution and formation of North Pacific Intermediate Water, J. Phys. Oceanogr., 23, 517-537, http://doi.org/10.1175/1520-0485(1993)023<0517:dafonp>2.0.co;2, 1993.
Talley, L. D.: North Pacific Intermediate Water transports in the mixed water region, J. Phys. Oceanogr., 27, 1795-1803, http://doi.org/10.1175/1520-0485(1997)027<1795:npiwti>2.0.co;2, 1997.
Tsunogai, S., Ono, T. and Watanabe, S.: Increase in total carbonate in the western North Pacific water and a hypothesis on the missing sink of anthropogenic carbon, J Oceanogr., 49, 305-315, http://doi.org/10.1007/bf02269568, 1993.
Wang, X., Ma, H., Li, R., Song, Z. and Wu, J.: Seasonal fluxes and source variation of organic carbon transported by two major Chinese Rivers: The Yellow River and Changjiang (Yangtze) River, Global Biogeochem. Cycles, 26, GB2025, http://doi.org/10.1029/2011GB004130, 2012.
Ward, N. D., Bianchi, T. S., Medeiros, P. M., Seidel, M., Richey, J. E., Keil, R. G. and Sawakuchi, H. O.: Where carbon goes when water flows: Carbon cycling across the aquatic continuum, Front. Mar. Sci., 4, http://doi.org/doi:10.3389/fmars.2017.00007, 2017.
Wu, L., Cai, W., Zhang, L., Nakamura, H., Timmermann, A., Joyce, T., McPhaden, M. J., Alexander, M., Qiu, B., Visbeck, M., Chang, P. and Giese, B.: Enhanced warming over the global subtropical western boundary currents, Nat. Clim. Change, 2, 161-166, http://doi.org/10.1038/nclimate1353, 2012.
Wu, K., Dai, M., Li, X., Meng, F., Chen, J. and Lin, J.: Dynamics and production of dissolved organic carbon in a large continental shelf system under the influence of both river plume and coastal upwelling, Limnol. Oceanogr., 62, 973-988, http://doi.org/doi:10.1002/lno.10479, 2017.
Xu, C., Xue, Y., Qi, Y. and Wang, X.: Quantities and fluxes of dissolved and particulate black carbon in the Changjiang and Huanghe Rivers, China, Estuar Coast., 39, 1617-1625, http://doi.org/10.1007/s12237-016-0122-0, 2016.
Yang, D., Yin, B., Liu, Z., Bai, T., Qi, J. and Chen, H.: Numerical study on the pattern and origins of Kuroshio branches in the bottom water of southern East China Sea in summer, J. Geophys. Res.: Oceans, 117, C02014, http://doi.org/10.1029/2011JC007528, 2012.
Yang, D., Yin, B., Liu, Z. and Feng, X.: Numerical study of the ocean circulation on the East China Sea shelf and a Kuroshio bottom branch northeast of Taiwan in summer, J. Geophys. Res.: Oceans, 116, C05015, http://doi.org/10.1029/2010JC006777, 2011.
Yasuda, I.: Hydrographic structure and variability in the Kuroshio-Oyashio transition area, J Oceanogr., 59, 389-402, http://doi.org/10.1023/a:1025580313836, 2003.
Yasuda, I., Okuda, K. and Shimizu, Y.: Distribution and modification of North Pacific Intermediate Water in the Kuroshio-Oyashio interfrontal zone, J. Phys. Oceanogr., 26, 448-465, http://doi.org/10.1175/1520-0485(1996)026<0448:damonp>2.0.co;2, 1996.
Yasunaka, S., Nojiri, Y., Nakaoka, S.-i., Ono, T., Mukai, H. and Usui, N.: Monthly maps of sea surface dissolved inorganic carbon in the North Pacific: Basin-wide distribution and seasonal variation, J. Geophys. Res.: Oceans, 118, 3843-3850, http://doi.org/10.1002/jgrc.20279, 2013.
Yasunaka, S., Nojiri, Y., Nakaoka, S.-i., Ono, T., Whitney, F. A. and Telszewski, M.: Mapping of sea surface nutrients in the North Pacific: Basin-wide distribution and seasonal to interannual variability,

J. Geophys. Res.: Oceans, 119, 7756-7771, http://doi.org/10.1002/2014JC010318, 2014.

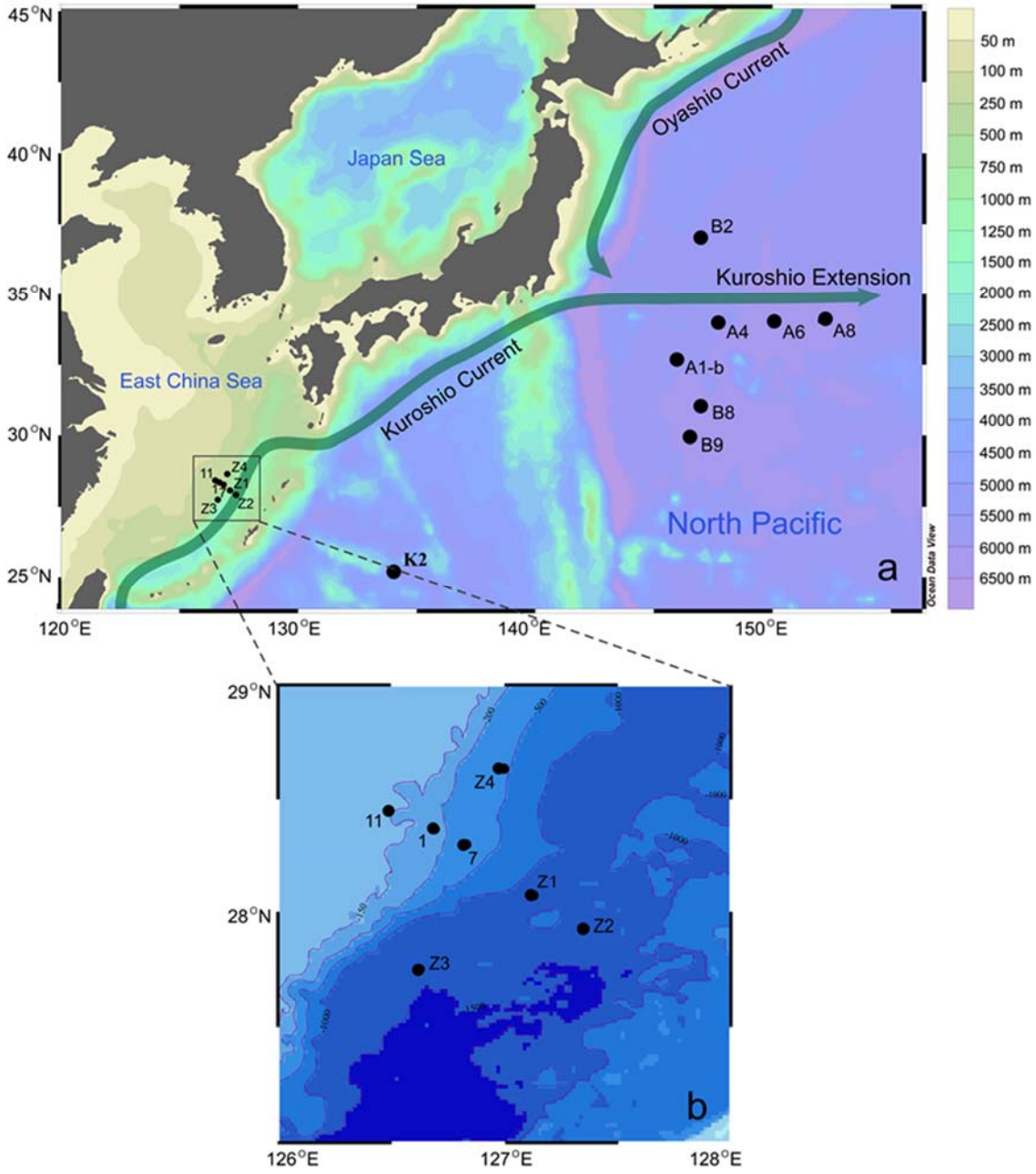

684

685 **Figure 1.** Map showing the study region and the sampling stations in the ECS and the
686 northwestern North Pacific (NP) during two cruises in 2014-2015 described in the text. Two
687 major western boundary currents, the northeastward-flowing Kuroshio and southward-flowing
688 Oyashio, meet and form the Kuroshio Extension (KE) flowing eastward to the North Central
689 Pacific (NCP).

690

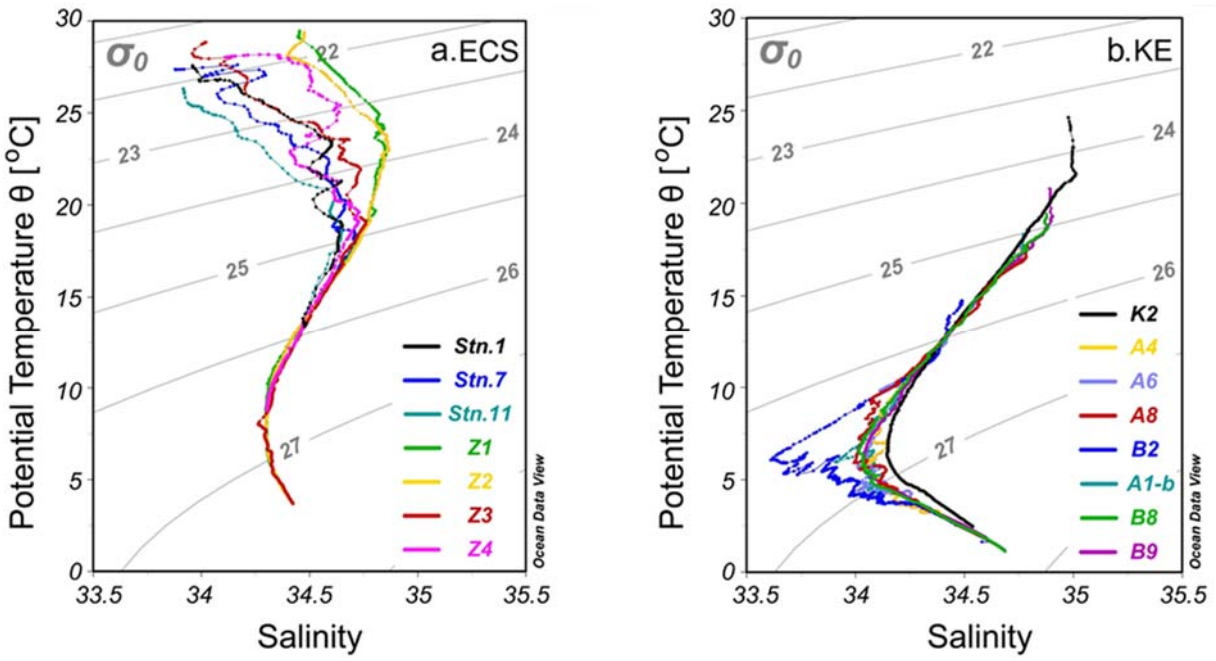

Figure 2. Potential temperature versus salinity plot (T-S) diagrams for the sampling stations. (a) Seven shelf-edge to slope stations in the ECS and (b) eight deep stations in the KE region in the northwestern NP.

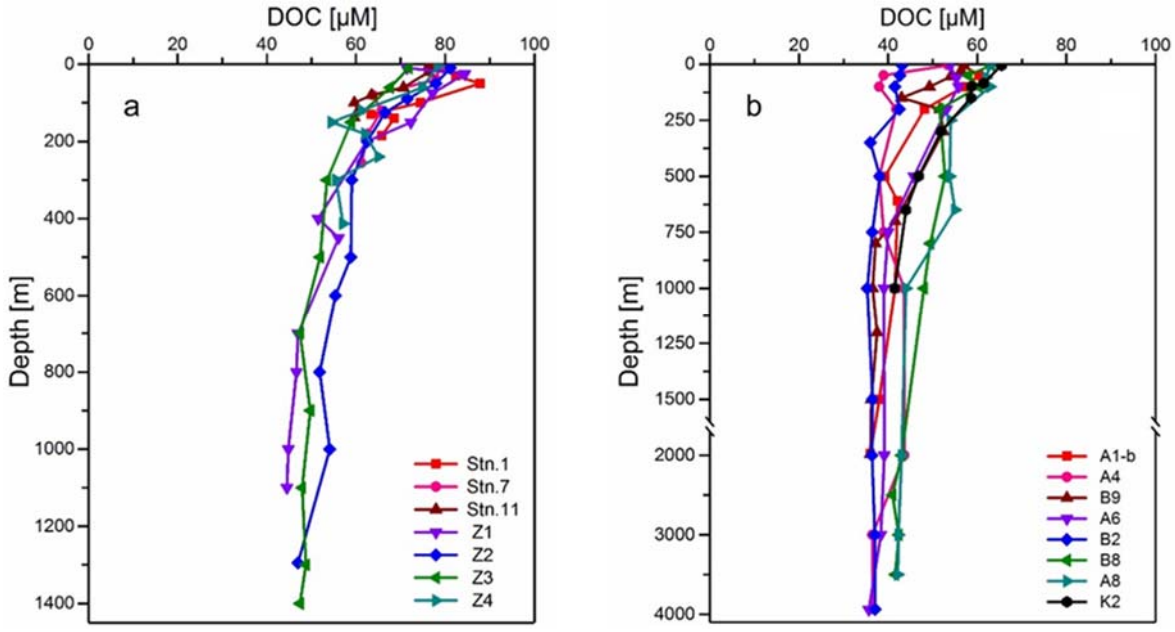

Figure 3. Depth profiles of DOC concentrations measured for the stations in the (a) ECS and (b) northwestern NP during the two cruises in 2014-2015. Note: The depth scale below 1500 m has been reduced in (b).

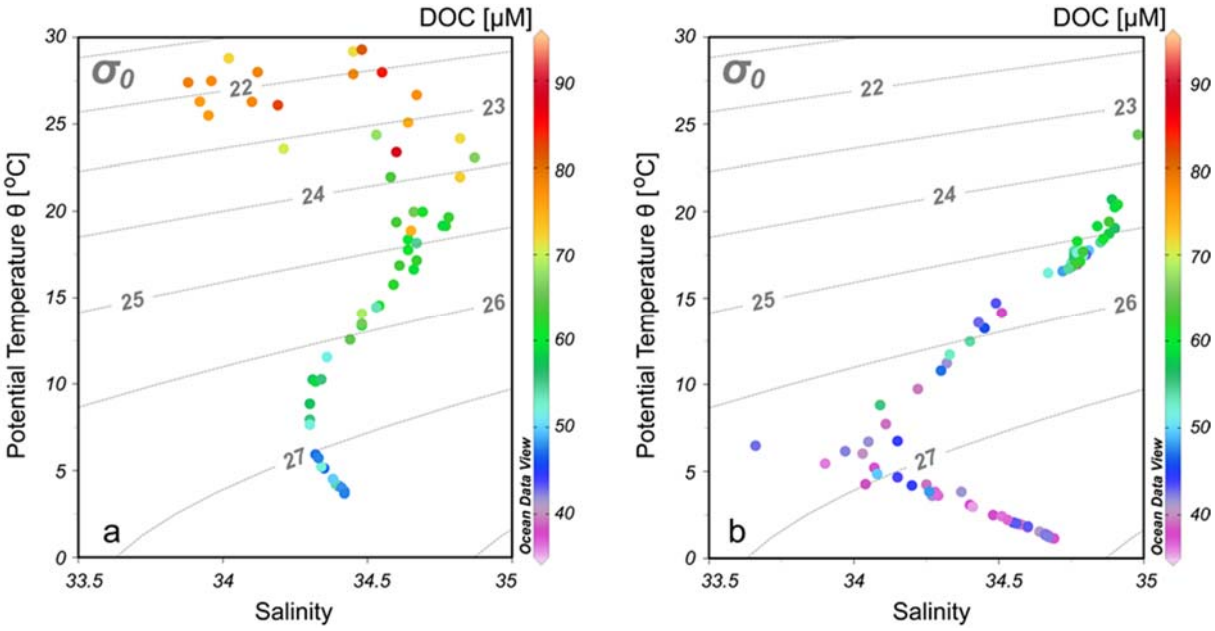

Figure 4. Field-observed DOC concentrations superimposed on plots of potential temperature versus salinity for the sampling stations in the (a) ECS and (b) Kuroshio Extension in the northwestern NP.

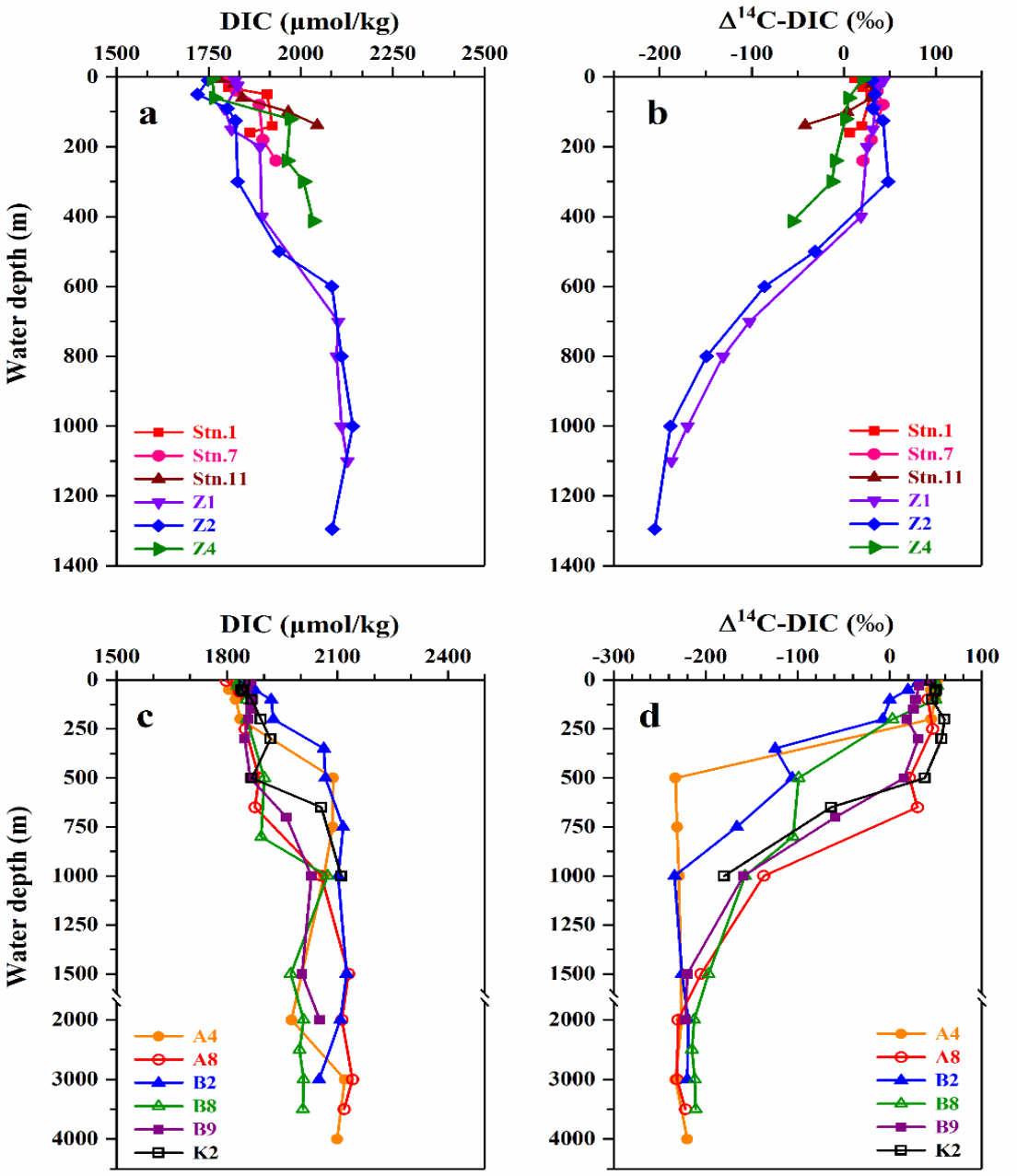

Figure 5. Depth profiles of DIC concentrations and Δ^{14}C-DIC measured for the stations in the (a, b) ECS and (c, d) northwestern NP during the two cruises in 2014-2015. Note: The depth scale below 1500 m has been reduced in (c and d). The plots were adapted from data previously reported in Ge et al. (2016) and Ding et al. (2018).

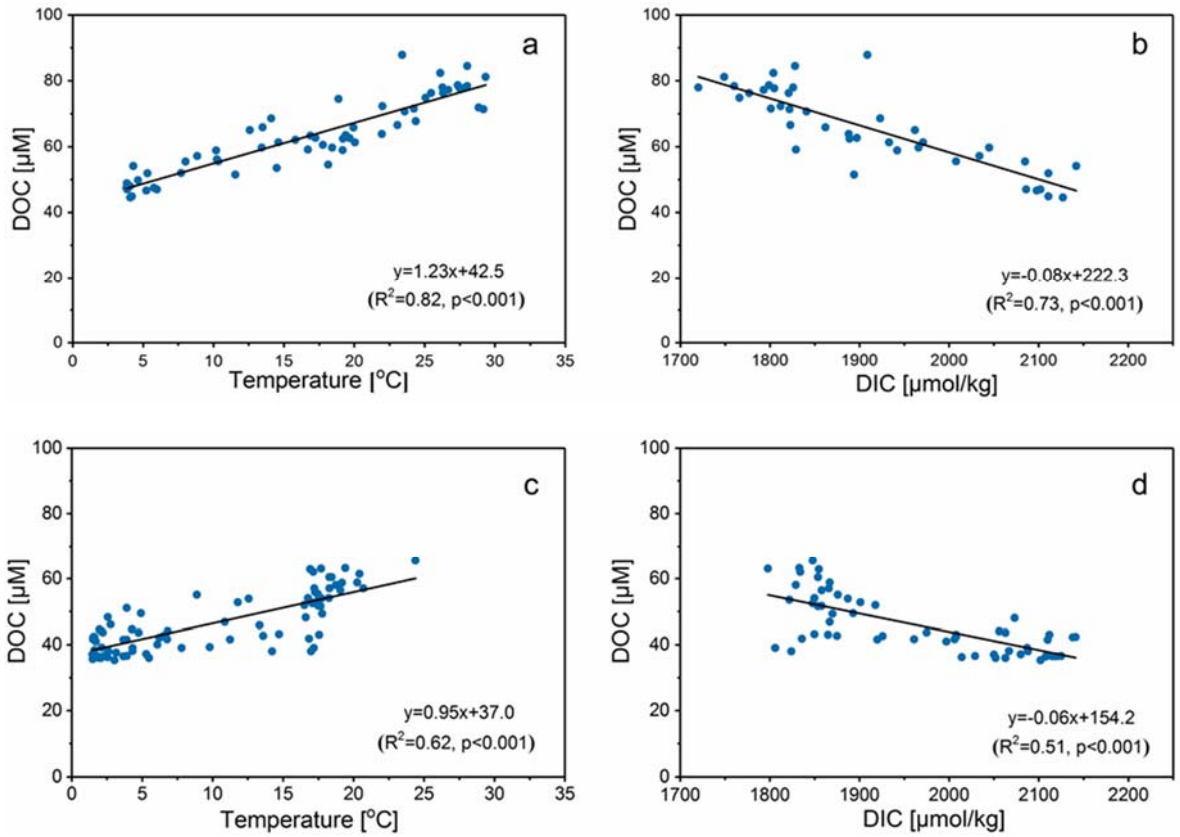

716

717 **Figure 6.** Correlation of DOC concentrations with water temperature and DIC concentrations
718 for stations sampled in the (a, b) ECS and (c, d) KE. The solid lines denote linear regressions
719 fit to the data.

720

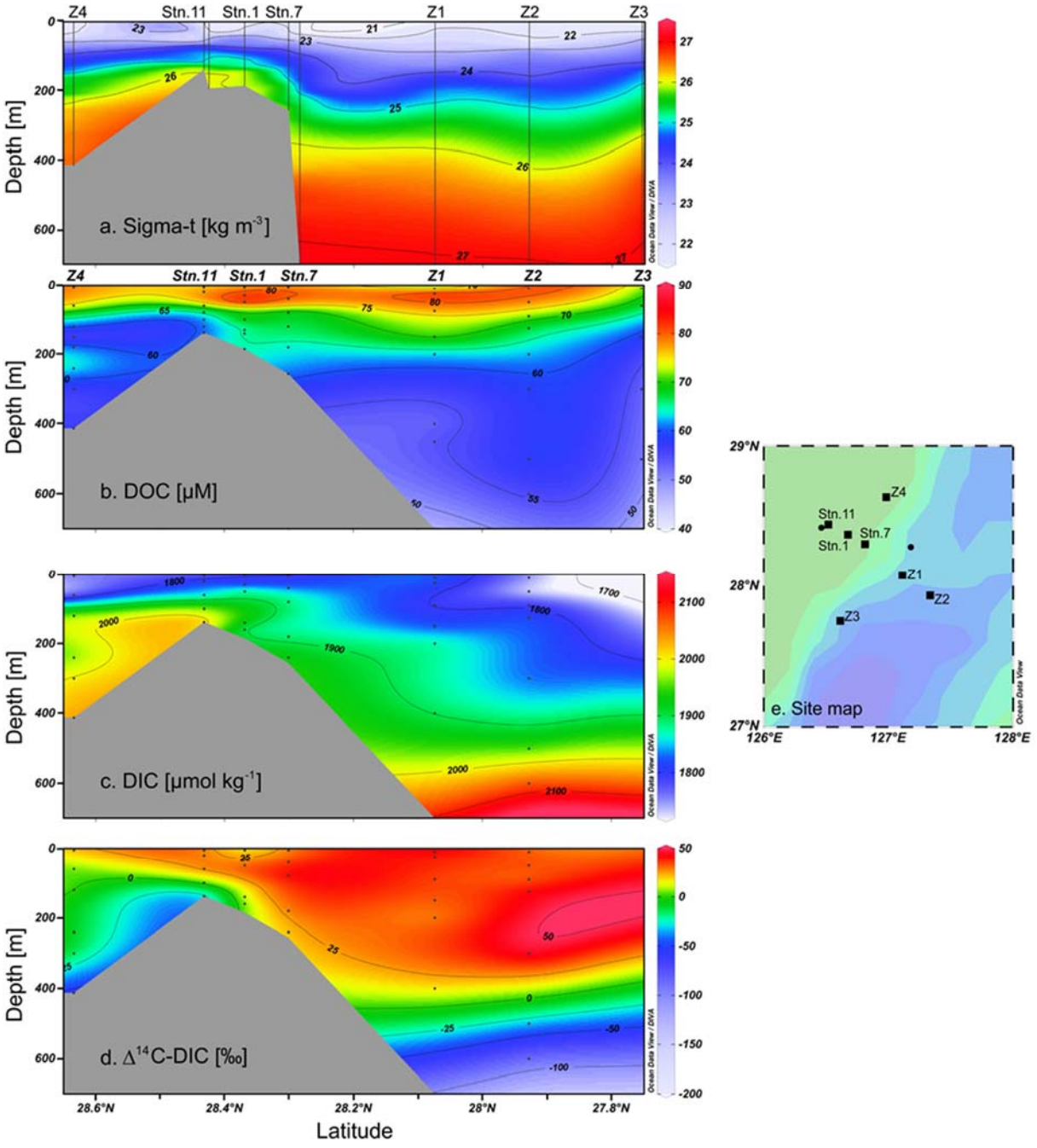

Figure 7. Transectional distributions of (a) density (Sigma-t, σ_t), (b) DOC concentrations, (c) DIC concentrations and (d) Δ^{14}C-DIC values for the (e) sampling stations (■) covering the shelf-edge and slope region of ECS during the cruise in July 2014. Black dots indicate the depths where samples were collected. Note: (a) The density of the other two stations (●) from the cruise in July 2011 are included to support the spreading of the data. (c-d) The distributions of density and DOC concentrations include seven stations, whereas DIC concentrations and Δ^{14}C-DIC values are given only for six stations due to the lack of data at Sta. Z3 (Ge et al., 2016).

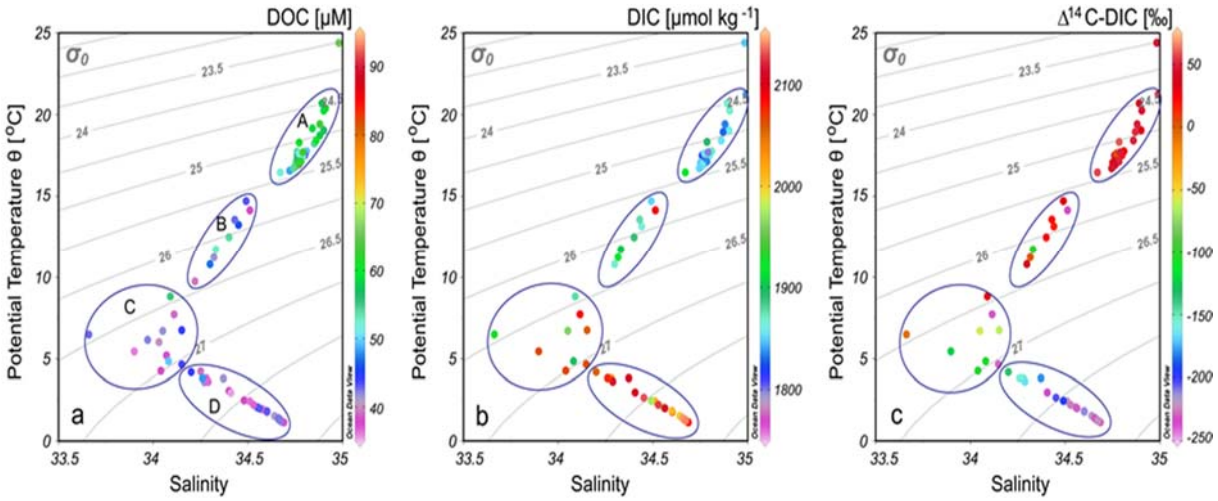

Figure 8. Plot of potential temperature (θ) *vs.* salinity with (a) DOC concentrations, (b) DIC concentrations and (c) Δ^{14}C-DIC values (indicated as the colours of points) associated with the potential water density (σ_t) for eight stations in the northwestern North Pacific (NP). The circular areas represent different water masses in terms of (A) lower density water in the upper 300 m depth with higher DOC concentration, lower DIC concentration and enriched Δ^{14}C-DIC; (B) mixed upper water in the 300-500 m depth; (C) mixed intermediated water in 500-800 m water depth; and (D) denser NP deep water below 1000 m depth. Note: DOC concentrations were measured for all stations, whereas DIC results from Ding et al. (2018) were only measured for six stations except Stas. A1-b and A6.

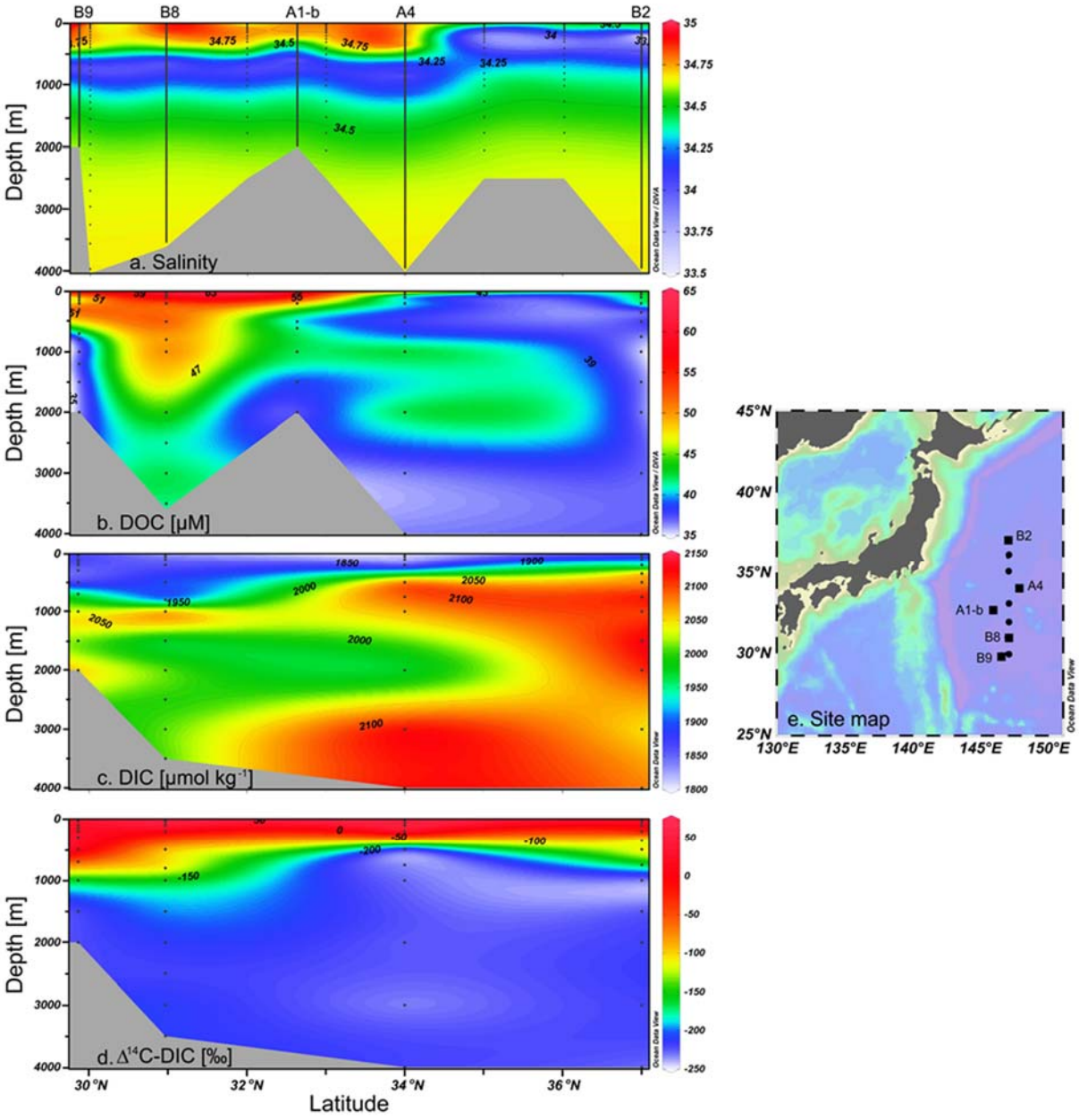

Figure 9. Transectional distributions of (a) salinity, (b) DOC concentrations, (c) DIC concentration and (d) Δ^{14}C-DIC values for (e) stations (■) sampled across the Kuroshio Extension (KE) in the northwestern NP. Black dots indicate depths where samples were collected. Note: (a) The salinity of another five stations (●) along the 35°N transect are included to support the spreading of the data. The hydrographic data for the five reference stations are taken from the Pacific data source in https://www.nodc.noaa.gov/ocads/. (c-d) DIC concentrations and Δ^{14}C-DIC values are given only for four stations due to the lack of data at Sta. A1-b (Ding et al., 2018).

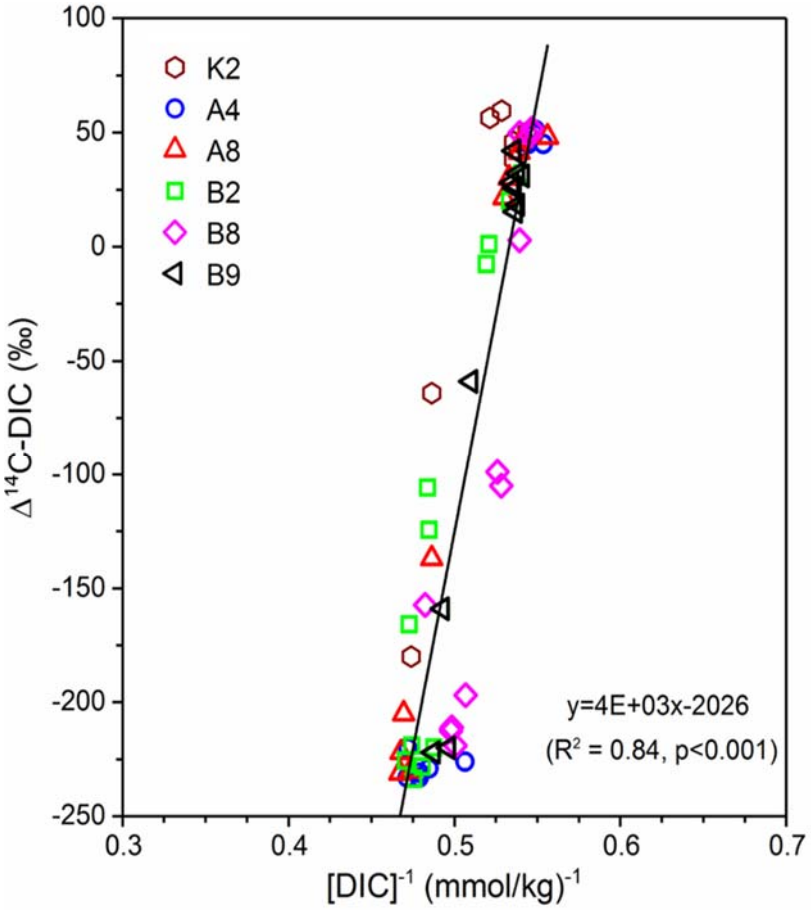

Figure 10. Keeling plot of Δ^{14}C-DIC *vs.* concentration of $[DIC]^{-1}$ measured for six stations (B9, B8, A4, A8, B2 and K2) in the northwestern NP (data from Ding et al. (2018)). The line indicates the linear regression fit to all data points.